Received: 18 September 2018 | Revised: 26 November 2018 | Accepted: 12 December 2018

DOI: 10.1002/wat2.1336

WILEY WIREs WATER

PRIMER

A primer on turbulence in hydrology and hydraulics: The power of dimensional analysis

Gabriel Katul[1] | Dan Li[2] | Costantino Manes[3]

[1]Nicholas School of the Environment, Duke University, Durham, North Carolina

[2]Department of Earth and Environment, Boston University, Boston, Massachusetts

[3]DIATI—Department of Environment, Land and Infrastructure Engineering, Torino, Italy

Correspondence Gabriel Katul, Nicholas School of the Environment, Duke University, Durham, NC 27708.
Email: gaby@duke.edu

Funding information
Army Research Office, Grant/Award Number: W911NF-18-1-0360; Compagnia di San Paolo, Grant/Award Number: Attrarre Docenti di Qualit tramite Starting Grant; Division of Atmospheric and Geospace Sciences, Grant/Award Number: NSF-AGS-1644382; Division of Earth Sciences, Grant/Award Number: NSF-EAR-1344703; Division of Integrative Organismal Systems, Grant/Award Number: NSF-IOS-1754893

The apparent random swirling motion of water is labeled "turbulence," which is a pervasive state of the flow in many hydrological and hydraulic transport phenomena. Water flow in a turbulent state can be described by the momentum conservation equations known as the Navier–Stokes (NS) equations. Solving these equations numerically or in some approximated form remains a daunting task in applications involving natural systems thereby prompting interest in alternative approaches. The apparent randomness of swirling motion encodes order that may be profitably used to describe water movement in natural systems. The goal of this primer is to illustrate the use of a technique that links aspects of this ordered state to conveyance and transport laws. This technique is "dimensional analysis", which can unpack much of the complications associated with turbulence into surprisingly simplified expressions. The use of this technique to describing water movement in streams as well as water vapor movement in the atmosphere is featured. Particular attention is paid to bulk expressions that have received support from a large body of experiments such as flow-resistance formulae, the Prandtl-von Karman log-law describing the mean velocity shape, Monin-Obukhov similarity theory that corrects the mean velocity shape for thermal stratification, and evaporation from rough surfaces. These applications illustrate how dimensional analysis offers a pragmatic approach to problem solving in sciences and engineering.

KEYWORDS
Buckingham π theorem, dimensional analysis, hydraulics, hydrology, turbulence

1 | INTRODUCTION

Hydrology and hydraulics are primarily concerned with water movement in liquid or vapor phases within natural (e.g., watersheds, wetlands and marshes, atmosphere) or engineered (e.g., pipes, ducts, channels, spillways) systems. In many instances, the water movement appears to be dominated by complex swirling or eddying motion that is labeled "turbulence." It is a flow state, not a fluid property, that is commonly contrasted with the simpler "laminar" flow state. At the microscopic level, the occurrence of turbulence may superficially appear to violate the second law of thermodynamics. How can so many water molecules spontaneously start to move almost coherently together in a large swirl or plume within eddies instead of following their random (or Brownian) motion trajectory predicted by the kinetic theory? The answer to this question is at the heart of turbulence research and has numerous consequences in a plethora of sciences. Flow organization by the swirling or eddying motion at some spatial scales leads to enhanced overall dissipation of energy (a conversion of kinetic energy to heat per unit time) by the action of viscosity (or internal friction in fluids), thus ensuring maximum entropy production. This assertion implies that order or coherency may be needed in certain regions of the flow domain to increase overall disorder or entropy in the entire flow domain. At the macroscopic (or continuum) level, water flow in a turbulent state can be described

by the momentum conservation equations, which are known as the Navier–Stokes (NS) equations. The NS equations have been derived to account for the effects of viscosity in fluids thereby marking a major departure from the so-called Euler equations for ideal or frictionless fluids. The mathematical properties of the NS equations (existence of solutions and smoothness) continue to be one of the important open problems in mathematics as declared by the Clay Mathematics Institute. The NS equations, being equations describing fluid velocity in time at a given position, tend to "hide" the numerous scales involved in energy transfer and dissipation by viscosity. Numerical integration of the NS equations or some approximated version of them has been one of the drivers in the creation of a new branch in science known as computational fluid dynamics (CFD). CFD lead to remarkable developments in both computer hardware and an impressive suite of numerical algorithms for solving NS (Pope, 2000) or a more fundamental version of them routed in molecular dynamics (Succi, 2001). Simulations have come long ways since Lewis Fry Richardson first attempted numerical weather predictions (Richardson, 1922). While Richardson's simulations failed to provide superior weather predictions, they did spawn novel ideas about turbulence representation and were partly responsible for the discovery of chaos in weather (Lorenz, 1963). High-performance computing and CFD have now sufficiently matured to a point they are beginning to replace expensive laboratory experiments and field-scale testing in numerous branches of engineering. As early as 1949, von Neumann envisioned that supercomputers can help unravel the "mysteries" of turbulence. While mainly used for research purposes, direct numerical simulations (DNS) of the NS equations that utilize a variety of brute-force numerical integration techniques are conducted to visualize the intricate flow patterns created by turbulence. At first glance, the DNS results may seem highly chaotic but actually hide a great deal of coherency. In the meantime, experimental facilities and instrumentation development as well as fast imaging techniques are allowing exploration and visualization of turbulence in ways not imaginable 20 years ago. In fact, modern flumes, pipes, and wind tunnel facilities are a testament to the rapid progress made when referenced to the early facilities of O. Reynolds (in 1883) and L. Prandtl (in 1904).

Progress on turbulence theories have not experienced the rapid developments witnessed in simulations and experiments. It is now becoming a cliche to recite a long list of famed engineers, mathematicians, and physicists (e.g., Boussinesq, Feynman, Heisenberg, Kolmogorov, Kraichnan, Landau, Per-Bak, Prandtl, Taylor, von-Karman) who worked on turbulence without offering the same successes achieved in their respective fields. Practitioners and engineers have recognized that finite viscosity marks a major departure from Euler's equations and subsequently developed a suite of experiments and tactics to describe turbulent flows. In fact, hydraulics was born because of operational needs to describe water flow in situations not addressed by early hydrodynamics that primarily dealt with the mathematics of frictionless fluids. Thus, around the turn from the 19th to the 20th century onwards, a large number of semiempirical formulae have been independently introduced to describe turbulent flow properties in hydraulics, hydrology, sediment transport, and meteorology. These formulae remain the corner stone of textbooks and working professional tool-kits alike (Brutsaert, 2005; French, 1985; Willcocks & Holt, 1899). Their success at packing a large body of experiments dealing with flow conveyance in pipes and channels as well as momentum and scalar mixing in stratified boundary layers, explains their wide usage in hydraulics, atmospheric, and climate models today. They continue to serve as "work-horse" equations for flow and transport in natural systems operating at Reynolds numbers that are simply too large for DNS. Arriving at these equations from dimensional considerations is the main goal of this primer. The approaches taken here bypass the need to use or solve explicitly the NS equations yet the outcomes they offer do not contradict the NS equations. Dimensional analysis also offers an efficient way to plan and execute experiments that unfold general laws in situations where the laws cannot be derived from first principles. They are the most effective and pragmatic dimension-reduction technique (a technique that reduces a system of differential equations into fewer equations by preserving desirable features of their phase space) invented in science.

2 | WHAT IS TURBULENCE?

Technically, there is no precise definition of turbulence and only defining syndromes are identified to distinguish turbulence from other flows characterized by fluctuating changes in pressure and velocity (such as nonlinear waves). These defining syndromes must be simultaneously satisfied and include (Tennekes & Lumley, 1972):

1. Irregularity: Turbulent flows are sufficiently irregular that they make a purely deterministic treatment impossible (theoretically and experimentally). An example of this irregularity is shown in Figure 1 featuring water velocity measurements above a smooth channel bed in a flume and atmospheric velocity measurements above a grass-covered surface described elsewhere (G. Katul & Chu, 1998; G. Katul, Hsieh, & Sigmon, 1997).The causes of this irregularity is often attributed to sensitivity to initial conditions—meaning a small change in initial conditions gets amplified through the nonlinear terms in the NS equations. This amplification leads to differing detailed temporal patterns in any realization of a flow variable at a point despite similarities in the flow configuration. However, the statistics of the flow variables associated with the same flow configuration represented by the flow realizations remain the same. For this reason, describing turbulence is akin to

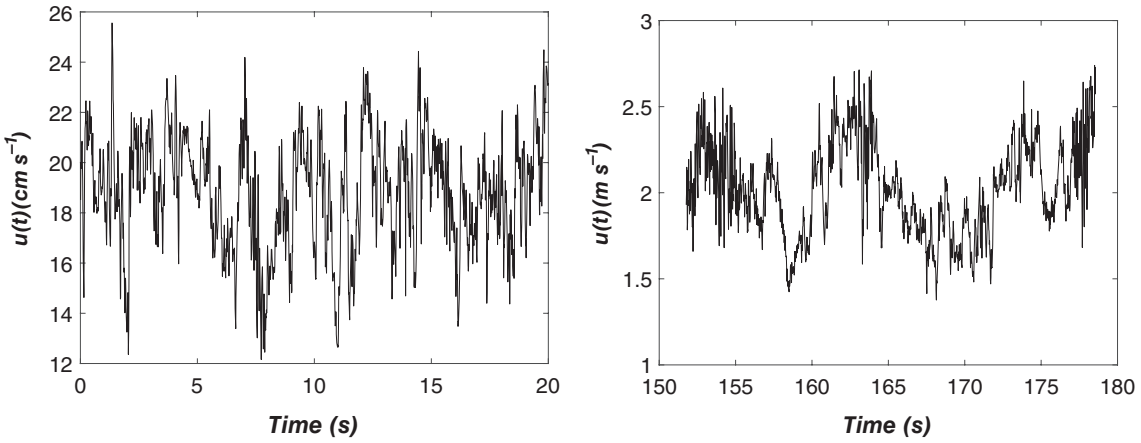

FIGURE 1 Measured longitudinal velocity time series $u(t)$ at $z = 1$ cm above a smooth open channel showing irregularity in turbulence (left). The measurements were sampled at 100 Hz when the water depth attained a uniform value of $h = 10$ cm. Measured $u(t)$ in the atmosphere at $z = 5$ m above a grass field (right) again illustrating similar irregularity to those reported in the smooth open channel flow. The measurements were sampled at 56 Hz during daytime conditions

describing the statistics of the flow variables as those appear to be "conserved" across repeated experiments with similar initial and boundary conditions. A highly simplified system illustrating the properties of such irregularity is the well-studied logistic map. The logistic map is defined as a recurrence relation (i.e., linking the variable at one time step in the future to the state of the variable in the present state) with a second-order nonlinearity and is archetypal of how chaotic behavior arises from a single nonlinear difference equation. It is used here to show (a) the chaotic nature of instantaneous solutions and (b) the preservation of statistics across similar initial conditions. The NS equations and the logistic map ($u(t+1) = -2u(t)^2 + 1$) can be expressed, respectively, as (Frisch, 1995)

$$\frac{\partial U_i}{\partial t} = -U_j \frac{\partial U_i}{\partial x_j} + \frac{\partial \tau_{ij}}{\partial x_j} + Bf_i, \tag{1}$$

$$u(t+1) - u(t) = -2u(t)^2 - u(t) + 1, \tag{2}$$

where $U_i = U_1, U_2, U_3$ are the instantaneous three velocity components that can also be interpreted as momentum per unit mass of fluid in direction x_i, $x_i = x_1, x_2, x_3$ are Cartesian coordinates, t is time, τ_{ij} are the overall viscous stresses and pressure P acting on a fluid surface given by

$$\tau_{ij} = \nu\left(\frac{\partial U_i}{\partial x_j} + \frac{\partial U_j}{\partial x_i}\right) - P\delta_{ij}, \tag{3}$$

and ν is the kinematic viscosity, $\delta_{ij} = 1$ when $i = j$ but is zero otherwise (the Kronecker delta), and Bf_i is an external force. Repeated subscript j implies summation from $j = 1$ to $j = 3$. The logistic map as arranged above shares the following with NS: (a) a velocity difference term (first term on the left-hand side) in time ($u(t+1) - u(t)$) approximating the local acceleration $\partial U_i/\partial t$, (b) a second-order nonlinear term (first term on the right-hand side), and (c) a term ($u(t)$) resembling a linear stress–strain expected from Newton's viscosity law for τ_{ij} (second term on the right-hand side), and a constant body force ($Bf_i = 1$) acting on the fluid (last term on the right-hand side). Figure 2 shows two solutions of the logistic equation determined by perturbing the initial condition $u(0) = 0.1$ with a small increment = 0.00001. After a certain period (only 100 steps shown), the two solutions diverge in time but their statistics, as quantified by the histogram or probability density function (PDF), remain the same.

2. Diffusivity: Turbulent flows are diffusive and efficient at transporting heat, mass, and momentum—at least when compared with their laminar counterparts.
3. Large Reynolds number: A large Reynolds number Re is necessary to ensure a turbulent flow state so that the aforementioned nonlinear inertia term (or advective acceleration term) in the NS equations far exceeds its viscous counterpart. The significance of this term is the main cause of irregularity as shown earlier. Formally and through a scaling argument applied to velocity gradients,

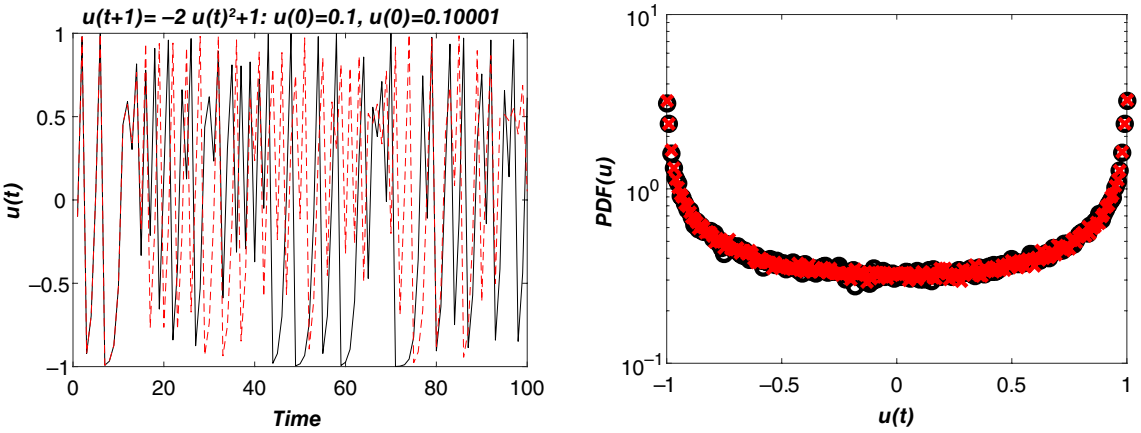

FIGURE 2 Two solutions for the logistic map differing only by a small perturbation in initial conditions (left). The histogram or probability density function (PDF) for the two solutions are also compared (right). Despite the differences in the temporal dynamics of the two solutions, their statistics (i.e., PDF) are virtually the same. These are the reasons why turbulence, which abides by Navier–Stokes (NS), is treated in a statistical manner

$$\mathrm{Re} = \frac{\left|U_j \frac{\partial U_i}{\partial x_j}\right|}{\nu\left(\frac{\partial^2 U_i}{\partial x_j \partial x_j}\right)} \sim \frac{Ul}{\nu} \quad \text{if} \quad |U_i| \sim U; \frac{\partial U_i}{\partial x_j} \sim \frac{U}{l}; \frac{\partial^2 U_i}{\partial x_j \partial x_j} \sim \frac{U}{l^2}. \tag{4}$$

Naturally, a transition from laminar (regular) to turbulent (irregular) flow occurs due to the growth of unstable modes that become energized and amplified by the nonlinear advective acceleration term (Drazin & Reid, 2004). The exact details of the transition to turbulence with increasing *Re* remains a subject of active research that is beyond the scope of this primer. Several highlights have been documented by an editorial in Nature Physics (Pomeau, 2016) as well as the influential and best-selling book on chaos (Gleick, 2011).

4. Three-dimensional vorticity fluctuations: This defining syndrome guarantees that turbulence is rotational and three dimensional. An important mechanism sustaining such vorticity fluctuation is vortex stretching originating from interactions between turbulent velocity and vorticity. Conservation of angular momentum requires that lengthening of vortices in three-dimensional fluid flow (vortex stretching) correspond to increases in the component of vorticity in the stretching direction. Vortex compression also occurs in turbulent flows. DNS has shown that while both stretching and compression occur, vortex stretching occurs more frequently (Pope, 2000). This velocity–vorticity interaction arises again from the advective acceleration term, which is quite large at high *Re*. Vortex stretching or compression is entirely absent in two-dimensional flows such as waves.
5. Dissipation and energy cascade: This defining mechanism distinguishes the energetics associated with the NS equations from the Euler equations. Viscous stresses always oppose velocity changes thereby acting to increase the internal energy of the fluid at the expense of kinetic energy of turbulence, also known as turbulent kinetic energy (TKE). In a nutshell, turbulence requires an external supply of energy that may be mechanical in nature (e.g., stirring, gravitational, or pressure gradients) or buoyant (as may be the case in convection or density gradients). Part of the external energy supply is used to generate pressure and velocity fluctuations over a wide range of time and spatial scales (i.e., TKE). Vortex stretching is then the main mechanism responsible for transferring TKE from large to small scales until it is dissipated into heat by frictional forces promoted by viscosity. Such kinetic energy loss rate is referred to as TKE dissipation rate or ϵ.
A Reynolds number *Re* can also be formulated to signify scale-wise separation between length scales where turbulence is produced (also referred to as integral scales L_I) and length scales where turbulence is dissipated by the action of viscosity and is referred to as the Kolmogorov microscale η. It is commonly assumed (Tennekes & Lumley, 1972) that the amount of TKE ($=\sigma_e^2$) produced at L_I is roughly balanced by the amount of kinetic energy dissipated at η. Hence, the production of TKE must scale as $\sigma_e^3/L_I \sim \epsilon$. The eddy sizes where the viscous dissipation rate occurs must include ν and ϵ and thus must scale as $\eta = (\nu^3/\epsilon)^{1/4}$. Combining these two findings results in $L_I/\eta \tilde{} Re_t^{\alpha}$ where $\alpha = 3/4$ and $Re_t = \sigma_e L_I/\nu$ is a Reynolds number formed from turbulent quantities. A high Re_t results in large separation between scales at which TKE is produced (i.e., L_I) and scales at which it is dissipated by the action of viscosity (i.e., η).On the topic of finite dissipation, another contrast to the Euler equations is the time irreversibility of NS. Time reversibility of equations of motion are often analyzed by substituting t with $-t$ and U with $-U$ (i.e., when reversing time, the velocity also reverses direction). For NS, the effect of this substitution can be traced through the following terms:

$$\frac{\partial(-U_i)}{\partial(-t)} = \frac{\partial U_i}{\partial t}, \text{(Time reversible)}, \tag{5}$$

$$-U_j \frac{\partial(-U_i)}{\partial x_j} = U_j \frac{\partial U_i}{\partial x_j}, \text{(Time reversible)}, \tag{6}$$

$$-\frac{\partial P}{\partial x_i} = -\frac{\partial P}{\partial x_i}, \text{(Time reversible)}, \tag{7}$$

$$\nu\left(\frac{\partial(-U_i)}{\partial x_j} + \frac{\partial(-U_j)}{\partial x_i}\right) = -\nu\left(\frac{\partial U_i}{\partial x_j} + \frac{\partial U_j}{\partial x_i}\right), \text{(Time irreversible)}. \tag{8}$$

Hence, the analysis here suggests that the viscous term delineating ideal ($\nu = 0$) from real ($\nu > 0$) fluids is one of the reasons why NS are time irreversible. Another reason is the chaotic nature of the flow that is conceptually similar to the deterministic chaos encountered in the logistic equation. Any slight variability in the description of $U_i(t_o)$ at a future time t_o results in time irreversibility. In chaotic systems, small variations amplify with the progression of time whether time is marching forward or backward. The NS and the Euler equations share this chaotic feature. Clearly, irregularity and time irreversibility are linked in NS despite the fact that the nonlinear advective acceleration term itself is time reversible.

6. Continuum: Turbulence is assumed to abide by the continuum assumption, meaning that fluid and flow properties such as density, temperature, pressure, viscosity, velocity, or energy can be defined at a "point." The term "point" here deviates from the conventional mathematical definition of a sphere with zero radius. In the continuum assumption, a "point" refers to a small volume whose radius is sufficiently large to encompass numerous molecules so that all fluid properties do not vary with variations in the size of the sphere. In turn, this radius must be sufficiently small to capture all the relevant gradients of flow properties. This assumption allows turbulence to be represented by the NS equations at a point already used here.

To sum up, the NS equations are the fluid-flow analog to Newton's second law in solid mechanics ($F = ma$, F is the net force imbalance acting on a solid object of mass m and a is its acceleration). Solving for the flow given by NS (i.e., U_i or some statistic of it) requires knowledge of the forces moving the fluid (e.g., pressure gradient, gravitational potential, etc...), the key fluid property needed to describe resistance to flow, geometric constraints on the flow such as the flow domain dimensions, and boundary conditions (e.g., roughness properties of the surface). Dimensional analysis takes full advantage of these basic ingredients to formulate plausible (i.e., dimensionally consistent) form of the solution to NS without actually solving the NS.

3 | DIMENSIONAL ANALYSIS

3.1 | Overview

J.W. Strutt, later known as Lord Rayleigh, prefaced his 1915 work on the principle of similitude (i.e., dimensional analysis) with this paragraph (Rayleigh, 1915): "*I have often been impressed with the scanty attention paid even by original workers to the great principle of similitude. It happens not infrequently that results in the form of laws are put forth as novelties on the basis of elaborate experiments, which might have been predicted a priori after a few minutes of consideration*". By no means is Lord Rayleigh the first to propose the use of dimensional analysis. In fact Galileo used the principle of similitude some 300 years earlier to reason that animals that grow in size while keeping the same shape cannot grow indefinitely (D'arcy, 1915). Galileo's argument rests on the fact that growth in weight scales as some l^3 (assuming constant density), whereas growth in strength must be related to some cross-sectional area transmitting forces, and thus must increase as l^2. This argument leads Galileo to conclude that the animal strength-to-weight ratio changes in proportion to l^{-1}, where l is some characteristic dimension most impacted by growth. Hence, larger animals have smaller strength-to-weight ratio. This argument would be rather difficult to envision without the power of dimensional analysis (Lemons, 2018).

So, what is dimensional analysis and how to implement it in the studies of turbulence in hydraulics and hydrology? Conveyance and transport laws describing turbulent flows must arrive at relations among physical variables that have dimensions of fluid mass [M], length [L], time [T], temperature [K] or scalar concentration [C]. Ideally, these relations must be derived from the NS equations, which remain elusive. Dimensional analysis attempts to arrive at those relations from the point of view of dimensional consistency (or homogeneity) supplemented by a fundamental theorem (Buckingham, 1914): the Buckingham

π theorem (BPT). In the applications of dimensional analysis, identifying all the variables impacting the sought quantity is the most challenging step. As earlier noted, the variables to be selected must include (a) constraints on the flow such as geometric constraints (i.e., domain size or other restrictive dimensions, distance from boundaries), (b) boundary conditions (e.g., roughness element size, surface heating, surface water vapor concentration), (c) fluid properties (e.g., density ρ, dynamic viscosity μ, or kinematic viscosity ν) usually needed to quantify internal resistance to flow, and (d) external forcing driving the flow (e.g., pressure gradients, gravitational potentials). Once the list of variables is identified, the BPT can be implemented through the following steps: First, the number of dimensionless groups ($= M_d - N_d$) is determined based on the number of variables listed ($= M_d$) and the number of independent units involved ($= N_d$). Second, the dimensionless groups (labeled as π) are formed based on the choice of repeat variables (also set to $= N_d$) and dimensional homogeneity. Third, one dimensionless group describing the flow variable of interest is written as a function of all the other dimensionless π groups usually in the form $\pi_1 = f(\pi_2, \pi_3, ..)$. The functional form of $f(.)$ needs to be determined experimentally. Occasionally, exploring limiting cases allows some aspects of the functional form of $f(.)$ to be partly unraveled. This tactic requires one of the π groups to approach zero or infinity thereby ensuring its overall contribution to $f(.)$ is a finite constant multiplier provided the remaining π groups are not small (Barenblatt, 1996). This approach is now illustrated through examples that are further discussed in the future reading section where the functional form of $f(.)$ may be derived from phenomenological theories. None of the formulae considered here has been directly derived from the NS equations. However, a growing number of studies that use results from DNS confirm that the expressions considered here are not inconsistent with the NS equations.

3.1.1 | Example 1: The Chezy equation and Manning's formula

One of the basic equations in stream or open channel flow links the flux of water (defined as the flow rate Q per unit area A normal to the flow direction) to the hydraulic radius $R_h = A/P_w$ (P_w is the wetted perimeter), the bed slope S_o, and a so-called empirical roughness coefficient. This equation is named after Antoine de Chezy (Chézy, 1775) and is considered the most lasting resistance formula to be derived from experiments.

To illustrate, consider a prismatic channel of length L_c characterized by a hydraulic radius R_h and surface roughness height r as shown in Figure 3. The hydraulic radius R_h is defined as the ratio of the cross-sectional area ($= Bh$) to the wetted perimeter ($B + 2\ h$). For a wide channel, $h/B << 1$ and $R_h = h/(1 + 2\ h/B) \approx h$. The roughness measure r may be related (but not equal) to the mean height of the protruding roughness elements distributed along the channel bed and its sides. Because the flow is assumed to be steady and uniform, the bulk (or area-averaged) velocity is equivalent to the water flux so that $V = Q/A$. This is the desired variable to be derived from dimensional considerations here. For this flow and channel geometry, Newton's second law can be used to link the driving force for water movement and the frictional resistance formed by a surface shear stress τ_o and the overall area over which this frictional stress acts. For small angle θ such that $S_o \approx \sin(\theta) \approx \tan(\theta)$, the force driving the flow down slope is, as noted in Figure 3, the weight of the water along the channel slope direction. Hence, the gravitational driving force is $F_g = mg\ \sin(\theta)$, where m is the fluid mass in the control volume ($= L_cBh$) and is given as ρL_cBh. The forces opposing F_g are side ($= 2\tau_o(L_ch)$) and bed ($= \tau_o(BL_c)$) frictional forces assumed to originate from the same frictional stress τ_o. For a steady and uniform (i.e., nonaccelerating) flow, the force balance yields

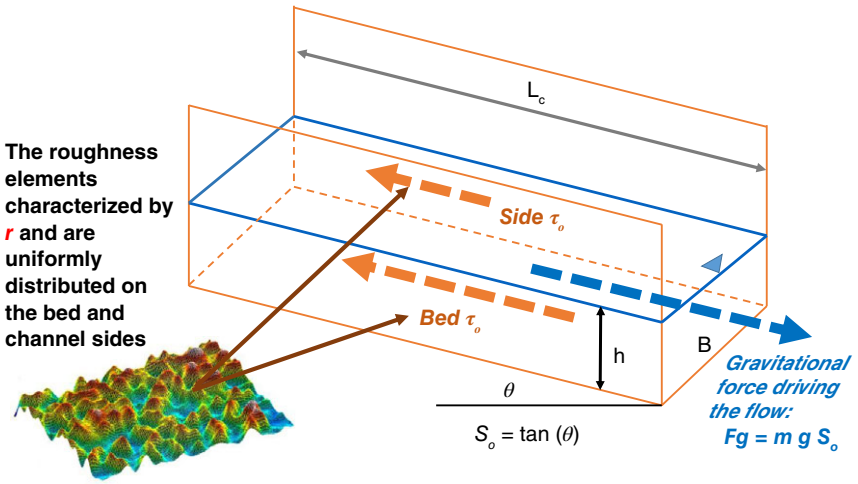

FIGURE 3 A uniform rectangular channel characterized by water depth h, width B, length L_c, slope S_o, and surface roughness characterized by a protrusion height r into the flow. The bed and one of the side stresses resisting the flow τ_o are shown along with the gravitational force F_g driving the flow along S_o

$$F_g = \rho(L_c B h) g S_o = \tau_o(B L_c) + 2\tau_o(L_c h), \tag{9}$$

$$\Rightarrow \tau_o = \rho(gSo) R_h. \tag{10}$$

Hence, the frictional stress τ_o can be uniquely determined from R_h, ρ, and gS_o. As noted earlier, the dimensional analysis here seeks to derive an expression for the desired variable V from the flow conditions and channel geometry. Because τ_o is a derived quantity, it need not be used in the analysis as an independent variable. To arrive at a list of variables impacting V from the most primitive variables, the following choices are made:

1. R_h for flow constraints,
2. r for boundary conditions at the channel bottom and side,
3. ρ and μ for fluid properties that are routinely combined to define a kinematic viscosity $\nu = \mu/\rho$ (also emerges in the viscous stress of the NS), and
4. gS_o for external forcing derived from the gravitational component driving the flow downslope, where g is the gravitational constant (and is connected to Bf_i in NS).

Hence, $V = f(R_h, r, \nu, gS_o)$, where $f(.)$ is an unknown function. Again, τ_o is not included in this list of variables given its complete dependence on ρ, g, S_o, and R_h that are all included in $f(.)$.

The application of the BPT proceeds as follows: Determine the

1. number of variables $M_d(= 5)$ (V, R_h, r, ν, gS_o).
2. number of units involved $N_d(= 2)$. Only $[L]$, $[T]$ are selected as $[M]$ has been eliminated by the choice of ν instead of μ and ρ.
3. number of dimensionless (or π) groups required: $M_d - N_d = 5–2 = 3$.
4. repeating variables $(= N_d = 2)$ to be common to all the dimensionless groups. It is convenient here to choose the repeating variables as forcing $(= gS_o)$ and geometric constraint $(=R_h)$. The choice of S_o and R_h is based on experimental pragmatism because they are convenient to measure when compared to other variables such as r.

Hence, based on the BPT, the three π groups with gS_o and R_h as repeating variables are:

$$\pi_1 = V(gS_o)^{a_1}(R_h)^{a_2}; \pi_2 = r(gS_o)^{a_3}(R_h)^{a_4}; \pi_3 = \nu(gS_o)^{a_5}(R_h)^{a_6}. \tag{11}$$

Determining a_1 and a_2 for π_1 proceeds as follows: noting that the dimensions of $V = [L][T]^{-1}$, $gS_o = [L][T]^{-2}$, and $R_h = [L]$ and that π_1 must be dimensionless results in the following algebraic equations:

$$\pi_1 = V(gS_o)^{a_1}(R_h)^{a_2} = [L][T]^{-1}\left([L][T]^{-2}\right)^{a_1}[L]^{a_3}; 1 + a_1 + a_2 = 0; -1 - 2a_1 = 0. \tag{12}$$

Hence, $a_1 = -1/2$ and $a_2 = -1 - a_1 = -1 + 1/2 = -1/2$. Repeating for π_2 and π_3 leads to $a_3 = 0$ and $a_4 = -1$, and $a_5 = -3/2$ and $a_6 = -1/2$. That is, $\pi_1 = f_1(\pi_2, \pi_3)$ yields

$$\frac{V}{\sqrt{gS_o R_h}} = f_1\left(\frac{r}{R_h}, \frac{\nu}{R_h\sqrt{gS_o h}}\right). \tag{13}$$

This expression is a relation between a Froude number $Fr = V/\sqrt{gS_o R_h}$, the relative roughness height r/R_h, and a certain type of bulk Reynolds number formed by $Re_F = R_h(\sqrt{gS_o R_h})/\nu$ or $Fr = f_1(r/R_h, Re_F)$. The Froude number is a dimensionless number defined by the ratio of the flow inertia to an external field (i.e., the gravitational field along the flow direction in the open channel flow here). The Reynolds number is expressed as $U_o L/\nu$, where U_o is a characteristic velocity $(= \sqrt{gS_o R_h}$ here), L is a characteristic length $(= R_h$ here), and ν is the kinematic viscosity of water as before. The conventional or text-book version of the Chezy formula can now be stated as (Keulegan, 1938):

$$V = C_h\sqrt{R_h}\sqrt{gS_o}, \tag{14}$$

where C_h is the Chezy roughness coefficient and must vary as $C_h = f_1(r/R_h, Re_F)$. Dimensional analysis is unable to fully determine $f_1(.)$ necessitating its determination via experiments. However, in the limit of high Re_F, it is expected that C_h becomes independent of $Re_F^{-1}(\to 0)$, a state referred to as fully rough because the roughness elements protrude well above the viscous sublayer (a thin layer of fluid in direct proximity of the roughness elements, where the fluid flows in a laminar state; see next section) thereby simplifying the expression for C_h to be dependent only on r/R_h. Experiments in fully rough pipes and channels suggest a $C_h \sim (r/R_h)^{-1/6}$ over some range of r/R_h (but not all), where the $-1/6$ exponent is commonly referred to as the Strickler scaling whose origin and connection to other aspects of turbulence are discussed elsewhere (Bonetti,

Manoli, Manes, Porporato, & Katul, 2017; Gioia & Bombardelli, 2002). When this experimental result for C_h is combined with the Chezy equation,

$$V \sim \left(\frac{r}{R_h}\right)^{-1/6} \sqrt{gS_oR_h}, \tag{15}$$

which recovers the widely used Manning formula

$$V = \frac{1}{n} R_h^{2/3} S_o^{1/2}, \tag{16}$$

with $n \sim g^{-1/2} r^{1/6}$ (Manning, 1891). For historical reasons, Equation 15 is not used thereby making published values of n dimensional (Chow, 1959). This section commenced with an estimate of τ_o from Newton's second law, which is now used to provide an interpretation of C_h. Equation 17 can be written as

$$\frac{V^2}{R_h g S_o} = \frac{V^2}{\tau_o/\rho} = \frac{V^2}{u_*^2} = C_h^2, \tag{17}$$

where $u_* = (\tau_o/\rho)^{1/2}$ is the so-called friction (or shear) velocity defining a kinematic stress. This outcome shows that squared Chezy coefficient may be interpreted as an inverse drag coefficient thereby completing the sought result.

3.1.2 | Example 2: The law of the wall

While the previous section considered the bulk velocity V, the focus now is on the shape of the mean velocity profile $u(z)$, where z is the distance from the boundary and $V \approx (1/h)\int_0^h u(z)dz$.

Figure 4 shows the flow configuration associated with this example. In this case, the variable describing the geometric constraint on the flow is z, the boundary condition remains r, the most relevant fluid property is, as before ν characterizing internal friction, and the forcing is now surrogated to the wall stress τ_o. As earlier noted, this frictional stress arises to counter any driving forces as earlier encountered in the Manning–Chezy formula in uniform open channel flows. Also, as noted earlier in the interpretation of C_h, τ_o can be normalized by ρ so that kinematic units are used for stresses thereby eliminating $[M]$. The quantity $u_*^2 = \tau_o/\rho$, the squared friction velocity earlier defined, must be viewed here as a kinematic representation of the surface stress that depends on the external driving force and a fluid property. Dimensional analysis is now used to explore the function $f(.)$ in

$$\frac{du}{dz} = f(z, r, \nu, u_*). \tag{18}$$

As before, $M_d = 5$ and $N_d = 2$ necessitating three π groups. Repeating variables are selected as z and u_* representing, once again, the constraint and the forcing. The three π groups are:

$$\pi_1 = \frac{du}{dz} u_*^{a_1} z^{a_2}; \pi_2 = r u_*^{a_3} z^{a_4}; \pi_3 = \nu u_*^{a_5} z^{a_6}. \tag{19}$$

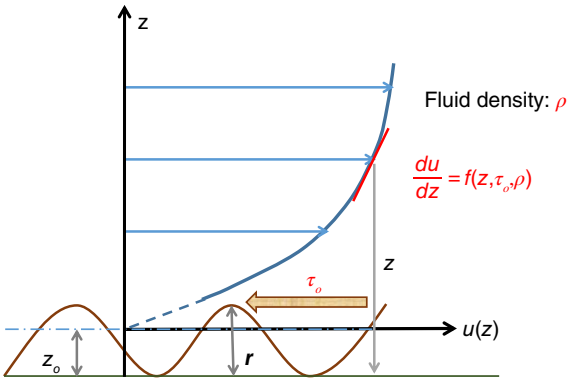

FIGURE 4 The variables impacting the mean velocity gradient du/dz. These include the height from the ground z, and the kinematic surface stress $u_* = \sqrt{\tau_o/\rho}$. As z increases, du/dz visually decreases. Also, in the limit of $\tau_o = 0$, $du/dz = 0$. Because τ_o is determined from a balance between frictional forces resisting the driving forces to ensure no acceleration, a $\tau_o = 0$ either implies no forcing (i.e., the flow is not moving) or a "free slip" condition. In the free slip condition, the flow no longer senses the presence of the surface and the velocity is finite at the surface

The dimensions of du/dz is $[T]^{-1}$, u_* is $[L][T]^{-1}$, r is $[L]$, and ν is $[L]^2[T]^{-1}$. Those dimensions are now used to determine $a_1....a_6$. For example,

$$\pi_1 = [T]^{-1}\left([L][T]^{-1}\right)^{a_1}[L]^{a_2}; -a_1 - 1 = 0; a_1 + a_2 = 0, \tag{20}$$

resulting in $a_1 = -1$ and $a_2 = 1$. Again, repeating this procedure to π_2 and π_3 yields $a_3 = 0$, $a_4 = -1$, $a_5 = -1$, and $a_6 = -1$. The dimensionless π groups are now expressed as:

$$\pi_1 = \frac{du}{dz}\frac{z}{u_*}; \pi_2 = \frac{r}{z}; \pi_3 = \left(\frac{u_* z}{\nu}\right)^{-1}. \tag{21}$$

Hence,

$$\frac{du}{dz}\frac{z}{u_*} = f\left(\frac{r}{z}, \frac{1}{Re_+}\right). \tag{22}$$

Again, π_3 is related to a Reynolds number $Re_+ = u_* z/\nu$ and π_2 resembles a local relative roughness. If ${Re_+}^{-1}$ is sufficiently small ($<< 1$) and the goal is to evaluate du/dz far from the wall boundary (i.e., $r/z << 1$), then $f(\pi_2, \pi_3)$ becomes independent of both π_2 and π_3 as these variables must saturate to some constant with ${Re_+}^{-1}$, $r/z \to 0$. Hence, $f(.)$ must be a constant far from the boundary and at large Re_+. That is,

$$\frac{du}{dz}\frac{z}{u_*} = \frac{1}{\kappa}. \tag{23}$$

Upon integration with respect to z,

$$u(z) = \frac{u_*}{\kappa}\log(z) + C_1. \tag{24}$$

Dimensional analysis alone cannot predict the numerical values of C_1 or κ. Experiments suggest that $\kappa \approx 0.4$ and this constant is known as the von Karman constant (Pope, 2000). Based on the variables impacting $f(.)$, the integration constant C_1 must be linked to the roughness element height r or the viscous sublayer thickness ν/u_* or both depending on whether the flow is fully rough, smooth, or transitional. For the fully rough case, it is assumed that at a momentum roughness height $z_o \sim r$, $u(z_o) = 0$ allowing C_1 to be determined from $-(u_*/\kappa)\log(z_o)$ and the log-law becomes

$$u(z) = \frac{u_*}{\kappa}\log\left(\frac{z}{z_o}\right). \tag{25}$$

Similar arguments can be repeated to evaluate C_1 for the smooth case by replacing $z_o \sim r$ with $z_o \sim \nu/u*$ (the viscous sublayer thickness).

It is instructive to ask to what extent Manning's formula or the Strickler scaling are connected to the log-law derived here. If the log-law describes the entire mean velocity profile in streams (which it does not), then the two examples can be linked via

$$V = \frac{1}{h}\int_{z_o}^{h} u(z)dz = \frac{u_*}{\kappa}\log\left(\frac{h}{ez_o}\right). \tag{26}$$

In the case of open channel flow, a force balance analysis results in $u_* = \sqrt{gS_o h}$ so that

$$V = \sqrt{gS_o h}\frac{1}{\kappa}\log\left(\frac{h}{ez_o}\right). \tag{27}$$

For a range of $h/z_o >> 1$, it was shown elsewhere (G. Katul, Wiberg, Albertson, & Hornberger, 2002) that the log function can be approximated by a power law given as

$$\log\left(\frac{h}{ez_o}\right) \approx \frac{5}{2}\left(\frac{h}{ez_o}\right)^{\alpha_1}, \tag{28}$$

where $\alpha_1 = 1/7–1/6$. If so, then the Strickler scaling and Manning's formula are approximately recovered (Bonetti et al., 2017). Last, it is worth noting that the log-law description for $u(z)$ has been the subject of some controversy with other power-law expressions being proposed when ν is small but finite (Barenblatt & Chorin, 1998; G. G. Katul, Porporato, Manes, & Meneveau, 2013). This controversy will be touched upon in the section titled Further Reading.

3.1.3 | Example 3: Monin–Obukhov surface layer similarity theory

This example is a generalization of the log-law when thermal stratification controls the density gradients as may be encountered in atmospheric flows. Under those conditions, modifications to du/dz by surface heating or cooling cannot be ignored. Surface heating or cooling introduces an additional length scale in the list of variables, known as the Obukhov length L_o (Businger & Yaglom, 1971; Foken, 2006). It is related to the strength of mechanical production and the buoyant production or destruction of TKE. It emerges from the TKE budget when subjected to stationary and planar homogeneous flow conditions in the absence of mean vertical velocity and assuming all the third-order turbulent transport terms (i.e., terms involving the transport of turbulent fluxes and variances) are small. Under these idealized conditions, the TKE budget reduces to the following expression (Kaimal & Finnigan, 1994):

$$\epsilon = u_*^2 \frac{du}{dz} + \frac{g}{T_a} \frac{H_s}{\rho C_p}, \tag{29}$$

where ϵ ($[L]^2[T]^{-3}$) is the mean TKE dissipation rate due to the action of viscosity, T_a is mean air temperature [K], H_s is the surface sensible heat flux (energy per unit area per unit time), and C_p is the specific heat capacity of dry air at constant pressure. The two terms on the right-hand side are mechanical production (as it involves mean velocity gradients) and buoyant production (when $H_s > 0$) or destruction (when $H_s < 0$) of TKE. As with the kinematic representation of the surface stress $\tau_o = \rho u_*^2$, H_s can be expressed in kinematic units as $Q_s = H_s/(\rho C_p)$ ($[M][T]^{-1}[K]$). The "equilibrium" relation describing ϵ arises from a balance between the viscous dissipation rate, mechanical, and buoyant production (or destruction) of TKE and can be made nondimensional as

$$\epsilon \frac{\kappa z}{u_*^3} = \frac{du}{dz} \frac{\kappa z}{u_*} + \frac{\kappa z}{u_*^3} \frac{g}{T} Q_s = \frac{du}{dz} \frac{\kappa z}{u_*} - \frac{z}{L_o}. \tag{30}$$

Monin and Obukhov similarity theory (Monin & Obukhov, 1954) argues that L_o ($[L]$) is a new length scale that must be added to the list of dimensional variables impacting du/dz ($[T]^{-1}$). Then the previous analysis must be amended to only accommodate L_o, representing another forcing due to surface heating or cooling. If the focus is restricted to very high Reynolds numbers (i.e., $1/Re_+ << 1$) and far from the boundary so that $r/z << 1$, the revisions yield

$$\frac{du}{dz} = f_2(z, u_*, L_o), \tag{31}$$

where $f_2(.)$ is to be partly determined from the BPT. As before, $M_d = 4$ and $N_d = 2$ so that there are two dimensionless π groups and two repeating variables chosen again as z and u_* for consistency with Example 2. It can be verified that the two π groups must be:

$$\pi_1 = \frac{du}{dz} z^{(+1)} u_*^{(-1)}; \pi_2 = L_o z^{(-1)} u_*^{(0)}, \tag{32}$$

so that $\pi_1 = f_2(\pi_2)$ or

$$\frac{du}{dz} \frac{z}{u_*} = f_2\left(\frac{z}{L_o}\right). \tag{33}$$

When $|z/L_o| << 1$, then $f_2(.)$ approaches a constant $= 1/\kappa$ as before. Dimensional considerations alone cannot predict the shape of $f_2(.)$. Phenomenological theories can predict the shape of $f_2(.)$ once a link to the energetics of the flow is established as discussed in further reading.

3.1.4 | Example 4: Evaporation from rough surfaces

The movement of water vapor molecules from rough surfaces such as soils or crops by eddies into the atmosphere is of primary significance to a plethora of applications including hydrological and meteorological forecasting, irrigation planning, energy partitioning, and subsequent growth of the atmospheric boundary layer, to name a few. Evaporation here is viewed as an interfacial phenomenon dealing with transfer of water vapor molecules from a solid surface into the eddies characterizing the turbulent state in the atmosphere. Hence, it is instructive to explore how far the BPT can be "pushed" to arrive at an expression for the evaporation rate F_E. As earlier noted, the variables to be selected describing F_E must include (a) constraints on the flow, (b) boundary conditions, (c) fluid and scalar properties, and (d) external forcing driving the transport of both scalars and the fluid. A summary of these variables is listed in Figure 5.

An obvious choice for external driving force for any scalar flux (water vapor here) is the mean concentration difference ΔC between the surface and the approximately well mixed atmosphere above the surface whereas $u_* = \sqrt{\tau_t/\rho}$ serves as the driving force for air flow as before. For boundary conditions, the roughness size r is an obvious choice impacting the flow,

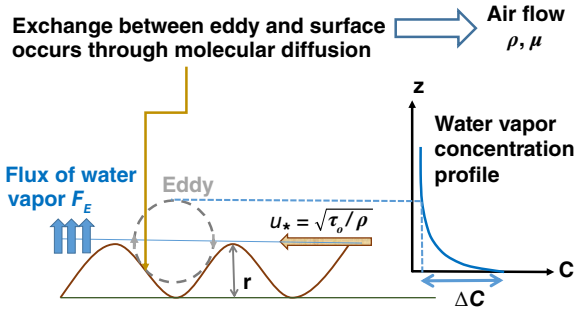

FIGURE 5 Evaporation rate or water vapor flux F_E from a bare soil surface characterized by a roughness r. The flow above the surface is an outcome of a balance between the driving forces and the frictional forces acting at the solid–air interface. The water vapor concentration at the surface and some distance from the surface is characterized by ΔC. The water vapor exchange between the moist roughness elements and the dry air aloft at the air–solid interface is only permissible through molecular diffusion. For this reason, the molecular diffusion coefficient of water vapor in air, D_m, is included in the analysis

also as before. For scalar and fluid properties, the molecular diffusivity of water vapor D_m (or any scalar such as heat) as well as kinematic viscosity ν of the transporting fluid (air here) are plausible choices. The constraints are not geometric dimensions here. They are implicitly specified given that F_E is representing water vapor transfer from an interface. That is, the analysis here assumes sufficient available energy from the environment to be present so that liquid water experiences a phase transition and water vapor molecules are produced at the interface to be transported from the surface. Stated differently, F_E is not limited by the energetics driving the phase transition but is governed by the efficiency of the mass transfer process. Based on this list of variables, it can be surmised that

$$F_E = f(\Delta C, u_*, D_m, \nu, r). \tag{34}$$

Hence, the use of the BPT to infer $f(.)$ proceeds as before. The number of variables $M_d = 6$, the number of units $N_d = 3$ ($[C]$, $[L]$, $[T]$). It is to be noted that the analysis here can be extended to sensible heat flux if the scalar selected is temperature instead of water vapor. In this extension, $[C]$ is replaced by $[K]$ with no additional modification. Hence, the number of dimensionless π groups is $M_d - N_d = 3$, and the number of repeating variables is $N_d = 3$. For pragmatic purposes, ΔC, u_*, and D_m are selected as repeating variables. Noting that the units of F_E are $[C][L][T]^{-1}$, ΔC is $[C]$, u_* are $[L][T]^{-1}$, D_m are $[L]^2[T]^{-1}$, ν are $[L]^2[T]^{-1}$, and r is $[L]$, it can be shown that

$$\pi_1 = F_E(\Delta C)^{-1}u_*^{-1}; \pi_2 = \nu/D_m = Sc; \pi_3 = ru_*/D_m. \tag{35}$$

Here, π_2 emerges as the molecular Schmidt number (named after E.H.W. Schmidt), which is close to unity for many gases in the atmosphere including water vapor ($Sc = 0.66$, 0.84, 0.99, 1.14, 1.22 for water vapor, carbon monoxide, methane, carbon dioxide, and sulfur dioxide, respectively). A similar analysis can be conducted for sensible heat and air temperature with the Prandtl number replacing the molecular Schmidt number (= 0.66 for temperature). Hence, the general expression for F_E becomes

$$F_E = \Delta C u_* f(Sc, ru_*/D_m). \tag{36}$$

While the BPT cannot predict the shape of $f(.)$, the fact that Sc does not vary appreciably for a given scalar such as water vapor in air allows simplifying the expression to

$$F_E = \Delta C u_* g_1(Sc) g_2(ru_*/D_m). \tag{37}$$

As earlier noted, some properties of g_2 may be further explored in certain limiting situations. In this case, the limiting situation is $r \sim \nu/u_*$ (i.e., r is related to the viscous sublayer thickness for smooth surfaces), then $g_1(.)$ and $g_2(.)$ both vary with Sc only. Hence, the BPT must predict $F_E = \Delta C u_* f(Sc)$ only. This expression is the text-book version of all bulk evaporation formulae predicting F_E to be linear in u_* (Brutsaert, 1982; Merlivat, 1978). Within the context of BPT, this finding also implies that $g_1(.)$ and $g_2(.)$ may be proportional to each other and vary with the same independent variable in the limit of smooth surfaces. Hence, to bridge the smooth and rough-surface formulations together, it may be convenient to redefine

$$F_E = \Delta C u_* g_3\left(Sc\frac{ru_*}{D_m}\right). \tag{38}$$

While the BPT argues that Sc and ru_*/D_m must be treated as independent, the limiting case of a smooth-wall being approached as $r \to 0$ suggest further simplifications. This simplification comes as possible lumping of π groups that could not

have been foreshadowed from dimensional considerations alone. For the rough case where $r >> \nu/u_*$ and assuming a plausible choice for $f(.)$ to be a power-law yields

$$F_E = A_E \Delta C u_* \left(Sc \frac{r u_*}{D_m} \right)^{n_e}, \tag{39}$$

where A_E is a similarity constant to be determined from experiments or theories (e.g., phenomenological). This power-law form was chosen so that when $r \sim \nu/u_*$, g_3 only varies with Sc^{n_e} and F_E remains $\propto \Delta C u_*$ for a given scalar characterized by its own molecular Sc. In general, n_e must also be determined from experiments or alternative theories. One such theory predicts $n_e = -1/4$ based on surface renewal schemes (Brutsaert, 1965) though this theory cannot predict A_E. Alternative phenomenological theories to surface renewal that make use of the energetics of turbulence also predict $n_e = -1/4$ and values to A_E (G. Katul & Liu, 2017a). These energetics are now the subject of the last example.

3.1.5 | Example 5: Kolmogorov's −5/3 law for the energy spectrum

In 1941, Kolmogorov published a deceptively simple formula describing the distribution of energy in eddies as a function of eddy sizes (Kolmogorov, 1941a, 1941b) and is hereafter referred to as K41. It was and remains one of the greatest successes of the use of dimensional analysis to unravel a complex phenomenon such as the distribution of turbulent energy in eddies. Hereafter, $E(k)$ represents the energy content (per unit mass) in eddies per unit wavenumber k, where k is inverse eddy size. K41 rests on the assumption that TKE production (P) at large scales (L_I) is balanced by energy transfer (T) across scales, which is then dissipated by the action of viscosity through ϵ at scales commensurate with η. The separation between L_I and η has been shown to vary with the Reynolds number ($L_I/\eta \tilde{} Re_t^{3/4}$). At scales for which this equilibrium condition (production P = transfer T = dissipation ϵ) holds, K41 reasoned that ϵ must be a conserved quantity as shown in Figure 6.

The common text book argument (Tennekes & Lumley, 1972) is that $E(k) = f(\epsilon, k)$. In this case, $M_d = 3$, $N_d = 2$, and the two repeated variables are ϵ and k. Hence, only one dimensionless group emerges from these choices and the BPT yields

$$\pi_1 = E(k) \epsilon^{a_1} k^{a_2} = \text{constant}. \tag{40}$$

The exponents a_1 and a_2 can be determined by noting that the dimensions of (a) $E(k)$ are $[L]^3[T]^{-2}$, (b) ϵ are $[L]^2[T]^{-3}$, and (c) k are $[L]^{-1}$. That is,

$$\pi_1 = [L]^3[T]^{-2} \left([L]^2[T]^{-3} \right)^{a_1} \left([L]^{-1} \right)^{a_2}; \; -3a_1 - 2 = 0, \; -a_2 + 2a_1 + 3 = 0. \tag{41}$$

Solving these equations yields $a_1 = -2/3$ and $a_2 = 3 + a_1 = 5/3$ and π_1 is now given by

$$\pi_1 = \frac{E(k)}{\epsilon^{2/3} k^{-5/3}} = C_k. \tag{42}$$

As before, dimensional analysis alone cannot determine the numerical value of the constant associated with π_1 but experiments suggest that this constant is $C_k \approx 0.55$ (Pope, 2000). In dimensional form, the celebrated K41 scaling law for the energy spectrum is given by

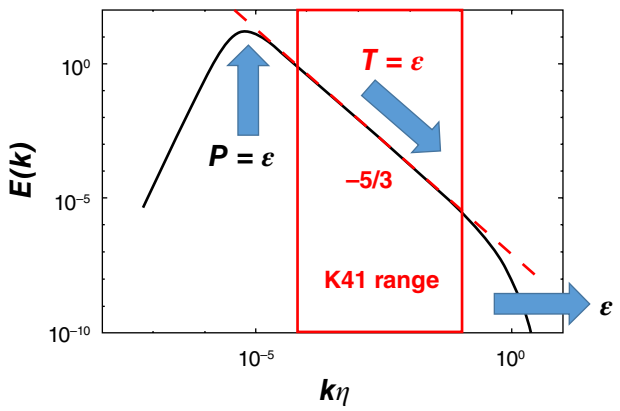

FIGURE 6 The shape of the energy spectrum $E(k)$ ($[L]^3[T]^{-2}$) as a function of wavenumber k ($[L]^{-1}$) or inverse of eddy sizes. K41 applies far from scales where energy is introduced (low k or large scales L_I) into the spectrum or removed by the action of fluid viscosity at small scales (or high k) commensurate to and smaller than η. Also, K41 assumes that the rate of energy production P, energy transfer across scales T, and TKE dissipation rate ϵ ($[L]^2[T]^{-3}$) are all equal. This assumption is labeled as "conservative" cascade—where the energy content varies across scales but the energy transfer rate ($P = T = \epsilon$) across k remains constant independent of k

$$E(k) = C_k \epsilon^{2/3} k^{-5/3}. \tag{43}$$

It has been demonstrated that the $k^{-5/3}$ scaling is associated with eddy sizes contributing to vortex stretching, one of the defining syndromes of turbulence. For this reason, occurrences of the $k^{-5/3}$ scaling in experiments have been associated with the presence of three-dimensional fully developed turbulence at high *Re*.

To bring this last point into focus, the $k^{-5/3}$ in K41 does not reflect any boundary conditions or fluid properties. To do so requires the use of BPT with the additional parameters of domain size L_d and ν. Using a similar approach to the prior examples, $E(k) = f(\epsilon, k, \nu, L_d)$. Hence, $M_d = 5$, $N_d = 2$, and upon selecting the repeated variables as in K41 (i.e., ϵ and k), the BPT results in

$$\pi_1 = \frac{E(k)}{\epsilon^{2/3} k^{-5/3}}; \pi_2 = \nu \epsilon^{a_3} k^{a_4}; \pi_3 = L_d \epsilon^{a_5} k^{a_6}. \tag{44}$$

Solving for $a_3..a_6$ yields the following: $a_3 = -1/3$, $a_4 = 4/3$, $a_5 = 0$, and $a_6 = 1$ and

$$\pi_2 = \nu \epsilon^{-1/3} k^{4/3}; \pi_3 = k L_d. \tag{45}$$

The π_2 already foreshadows the emergence of the Kolmogorov microscale given as $\eta = (\nu^3/\epsilon)^{1/4}$ and can be conveniently expressed as $\pi_2 = (k\eta)^{4/3}$. Hence,

$$E(k) = \epsilon^{2/3} k^{-5/3} f\left(kL_d, (k\eta)^{4/3}\right). \tag{46}$$

If η and L_d are sufficiently separated scalewise (i.e., $\eta/L_d \to 0$), then the function $f(.)$ can be decomposed into the product of two functions correcting K41 scaling at large ($kL_d \sim 1$) and small ($k\eta \sim 1$) scales. That is,

$$E(k) = \epsilon^{2/3} k^{-5/3} g_1(kL_d) g_2\left((k\eta)^{4/3}\right). \tag{47}$$

Again, BPT cannot predict $g_1(.)$ and $g_2(.)$. However, g_1 must encode the effects of boundary conditions on the shape of the spectrum at large scales, whereas g_2 may be more universal across various turbulent flows. This analysis also illustrates why K41 scaling can only hold for $k\eta << 1$ and $kL_d >> 1$ to ensure g_1 and g_2 attain constant values.

4 | FURTHER READING

Despite the successes of dimensional analysis in arriving at these empirical formulae, especially those describing the bulk (or macroscopic) flow and transport properties (Examples 1–4), what is evidently missing is the connection between them and the most prominent features of the flows they describe, namely, the turbulent energetics (or fluctuations) and eddies discussed in Example 5. Establishing the connection through phenomenological theories has been drawing significant research attention over the past 15 years, which is briefly discussed here. This topic is selected as further reading because it offers new tactics to infer $f(.)$ that are difficult to achieve via dimensional considerations alone. In certain instances, they offer connections between certain constants such as κ and C_o thereby providing additional constraints on the problem.

Phenomenological theories built on spectral links, cospectral budget models, and/or structure functions attempt to infer $f(.)$ from the universal character of $E(k)$ in Example 5. A seminal paper by Gioia and Bombardelli (2002) introduced a simplified version of the spectral link to arrive at Manning's formula and the Strickler's scaling (Example 1). Applications of this link to complex situations such as flows within emergent and submerged canopies followed with acceptable agreement between model calculations and measurements (Huthoff, Augustijn, & Hulscher, 2007; Konings, Katul, & Thompson, 2012). This approach was later expanded by relating the energetics of turbulent eddies to the Darcy–Weisbach friction factor f_{dw} (Brown, 2002, 2003) thereby explaining, for the first time, the shape of so-called Nikuradse curves (Gioia & Chakraborty, 2006) and Moody charts (Moody, 1944). The linkage between f_{dw} and $E(k)$ may be summarized as:

$$f_{dw} \propto \sqrt{\int_{1/l}^{\infty} E(k) dk}, \tag{48}$$

and was shown to be consistent with numerical solutions of detailed spectral budgets (Calzetta, 2009), where $l = r + a\eta$ is a characteristic scale that includes the surface roughness size r and the Kolmogorov microscale η as before. Equation 48 was verified using two-dimensional soap film experiments, where $E(k)$ was manipulated so as to scale as $k^{-5/3}$ or k^{-3} depending on whether the inverse energy cascade or forward enstrophy (or integral of vorticity) cascade applies (Guttenberg & Goldenfeld, 2009; Kellay et al., 2012; Tran et al., 2010). Another intriguing application of the relation between f_{dw} and $E(k)$ was the correct

inference of the intermittency exponent (Goldenfeld, 2006; Mehrafarin & Pourtolami, 2008) postulated by Kolmogorov's refinements to the inertial subrange scaling (Kolmogorov, 1962). To some degree, Equation 48 may be viewed as analogous to a fluctuation (i.e., related to $E(k)$)—dissipation (i.e., related to f_{dw}) phenomenological theory (Kubo, 1966) for turbulence (Goldenfeld & Shih, 2017). The spectral link was also used to highlight how f_{dw} may be enhanced above gravel beds at high Reynolds number due to eddy penetration into the porous medium and the resulting faster-than Darcy velocity within the gravel bed itself (Manes, Ridolfi, & Katul, 2012).

In another landmark study, Gioia and coworkers formalized their earlier approach to explain the entire shape of $u(z)$ above a smooth surface covered in Example 2 starting from an assumed shape of the spectrum of turbulent eddies (Gioia, Guttenberg, Goldenfeld, & Chakraborty, 2010). Their energy spectrum featured the well-established K41 scaling for inertial subrange eddies modified to include the effects of TKE generation at larger scales and viscous cutoff at smaller scales (see Equation 47) as shown in Figure 6. This approach was labeled the "spectral link" because it provides a link between the shape of the turbulent energy spectrum (i.e., fluctuations) to well-known features in the mean velocity profile (Gioia et al., 2010).

The spectral link was then employed to stratified atmospheric surface layer flows with the goal of deriving the so-called stability correction function to the mean velocity profile (see Example 3). Two modifications were necessary to implement the original spectral link to atmospheric flows: the inclusion of the effects of thermal stratification on the TKE mean dissipation rate and the eddy-size anisotropy (G. Katul, Konings, & Porporato, 2011). The resulting outcome provided a novel explanation for the power-law scaling exponents and coefficients in the stability correction function for momentum transfer. Thus, extensions of the spectral link to stratified atmospheric flows yielded fruitful connections between two separate theories developed by the Russian school of fluid mechanics: Kolmogorov's theory for inertial subrange eddies and Monin–Obukhov similarity theory requiring data-derived stability correction functions. It also explained the origin of the so-called OKEYPS equation (after Obukhov–Kazansky–Ellison–Yamamoto–Panofsky–Sellers) describing the stability correction function from near convective to mildly stable atmospheric flow (Foken, 2006). The stability correction functions have also been the subject of an "up-graded" dimensional analysis known as directional-dimensional analysis (Kader & Yaglom, 1990). Here, distinct velocities are used to normalize horizontal and vertical flow variables instead of only u_* offering a more plausible scaling to the intermediate region between neutral (no heating) and free convective (no shear) conditions.

Refinements were undertaken so as to relax some restrictions on the formulation of eddy-size anisotropy and to extend the aforementioned arguments to mean scalar quantities (G. Katul, Li, Chamecki, & Bou-Zeid, 2013; Li, Katul, & Bou-Zeid, 2012; Li, Salesky, & Banerjee, 2016; Salesky, Katul, & Chamecki, 2013). In the process of extending the spectral link to stratified turbulent flows, a number of limitations became apparent. The primary one is the oversimplified representation of the turbulent shear stress and associated momentum transfer (G. G. Katul, Porporato, et al., 2013), which is assumed to be dominated by a single scale of eddy motion motivated by the so-called attached eddy hypothesis (Townsend, 1976). The cospectral budget model was then developed to rectify this limitation, allowing for a new representation of the multiscale nature of turbulent transfer. The cospectral budget model recovers and refines the results obtained previously by the spectral link such as the mean velocity profile above a smooth surface (G. Katul & Manes, 2014; McColl, Katul, Gentine, & Entekhabi, 2016) and enables extensions to more complex situations as well as to scalar transport (G. Katul, Porporato, Shah, & Bou-Zeid, 2014; Li, Katul, & Bou-Zeid, 2015; Li, Katul, & Zilitinkevich, 2015; G. Katul, Li, Liu, & Assouline, 2016; Li et al., 2016; Li & Katul, 2017; McColl, van Heerwaarden, Katul, Gentine, & Entekhabi, 2017). It also offered a new perspective on the debate about the shape of the mean velocity profile (power-law versus log-law) as discussed elsewhere (G. G. Katul, Porporato, et al., 2013). This work showed that intermittency corrections to the spectrum of turbulence can lead, under some conditions, to power-law solutions for $u(z)$ even at infinite Re.

Phenomenological theories based on structure functions also explain the scaling laws in the evaporation from rough surface (see Example 4) when the gas transfer velocity linking F_E to ΔC is assumed to follow the K41 scaling subject to the viscous corrections derived from the von-Karman–Howarth Equation (G. Katul, Manes, Porporato, Bou-Zeid, & Chamecki, 2015), which is equivalent to assuming that eddies responsible for water vapor transfer at the air–surface interface scales with the Kolmogorov microscale. Such arguments successfully recover the "$-1/4$" scaling in Equation 39, which was derived in previous studies based on surface renewal theory (Brutsaert, 1965). The results suggest that the '$-1/4$' scaling law is an outcome of the Kolmogorov microscale and the associated time scale, while the viscous corrections only alter the scaling of F_E with respect to Sc but not u_* (G. Katul & Liu, 2017b). Revisions to surface renewal theories that account for large eddies have been proposed and reviewed elsewhere (G. Katul, Mammarella, Grönholm, & Vesala, 2018). These theories confirm that the similarity constant A_E in Equation 39 vary as power-law with a Reynolds number, a finding that has been confirmed by DNS and several laboratory studies (G. Katul et al., 2018).

Another interfacial phenomenon receiving renewed interest from phenomenological theories is fluvial hydraulics (Ali & Dey, 2018). The spectral link was recently used to explain a number of scaling laws reported experimentally regarding the incipient motion of sediment particles (Ali & Dey, 2017). It was shown that the densimetric Froude number, which describes

a dimensionless critical bulk velocity to initiate particle movement, can be linked to the submergence depth (r/h) via three scaling laws whose exponents are linked to $E(k)$. These links enlightened how the energetics of turbulence across various r/h alters the incipient motion of sediments.

5 | CONCLUSION

To conclude, recent advances in computational and experimental fluid mechanics have allowed for a greater understanding of many types of turbulent flows, which are universally considered as one of the main drivers of hydrological and hydraulic processes; despite these advances, hydraulics and hydrology practice has not effectively profited from them. Undoubtedly, the slow infusion of new knowledge into practice is related to the fact that mathematical treatment of turbulence as well as the understanding of its underpinning physics can be daunting and often accessible only to specialists. Fortunately, to ameliorate the situation, dimensional analysis has historically represented a powerful tool that, while bypassing the intricacies of turbulence theory, allows for the derivation of many formulae that are still routinely used in many problems of practical interest dealing with highly turbulent flows. This justifies the choice of the authors of writing a primer on turbulence specifically focused on dimensional analysis. However, a word of caution is in order here. The title of this primer should not fool the reader as dimensional analysis can be indeed a powerful tool but it should be considered by no means as the panacea for turbulent flows. After reading the present paper, the reader is now probably aware that significant results from dimensional analysis can be reached when the number of nondimensional groups governing the phenomenon is little and allows for the application of similarity principles. Moreover, the selection of these groups and governing variables requires deep understanding and intuition about the turbulent transport phenomenon. On the contrary, many problems in hydrology and hydraulics are governed by a large number of nondimensional groups, which makes it difficult to apply such principles and even to empirically explore functional relations among groups as these are heavily interlinked (Manes & Brocchini, 2015). As discussed in the previous section, another shortcoming of dimensional analysis is that it represents, by definition, a mathematical tool that is almost completely disconnected from the features of the flows it describes and, therefore, it is often bound to offer incomplete solutions that can be susceptible to scale issues. Lately, phenomenological theories based on the so-called spectral and cospectral budget approaches have offered an alternative to dimensional analysis to identify and recover laws of practical interest. The theoretical background to understand and apply such phenomenological approaches is clearly heavier when compared to dimensional analysis. Nonetheless they represent, to the authors' opinion, an exciting tool that may even accelerate the bridging between theory and practice in ways that still await discovery. For this reason, they are proposed as further reading to the reader seeking description of hydraulics and hydrology that goes beyond empirical laws.

ACKNOWLEDGMENTS

The authors thank A. Mrad, Y. Liu, and E. Zorzetto for helpful comments and suggestions. G.K. acknowledges support from the U.S. National Science Foundation (NSF-EAR-1344703, NSF-AGS-1644382, and NSF-IOS-1754893). D.L. acknowledges support from the U.S. Army Research Office (W911NF-18-1-0360). C.M. acknowledges support from "Compagnia di San Paolo" (project: "Attrarre Docenti di Qualità tramite Starting Grant").

CONFLICT OF INTEREST

The authors have declared no conflicts of interest for this article.

RELATED WIREs ARTICLES

The hydraulic description of vegetated river channels: the weaknesses of existing formulations and emerging alternatives
Life in turbulent flows: interactions between hydrodynamics and aquatic organisms in rivers

REFERENCES

Ali, S. Z., & Dey, S. (2017). Origin of the scaling laws of sediment transport. *Proceedings of the Royal Society A*, *473*(2197), 20160785.

Ali, S. Z., & Dey, S. (2018). Impact of phenomenological theory of turbulence on pragmatic approach to fluvial hydraulics. *Physics of Fluids*, *30*(4), 045105.

Barenblatt, G. (1996). *Scaling self-similarity, and intermediate asymptotics*. Cambridge, England: Cambridge University Press.

Barenblatt, G., & Chorin, A. J. (1998). New perspectives in turbulence: Scaling laws, asymptotics, and intermittency. *SIAM Review*, *40*(2), 265–291.

Bonetti, S., Manoli, G., Manes, C., Porporato, A., & Katul, G. (2017). Manning's formula and Strickler's scaling explained by a co-spectral budget model. *Journal of Fluid Mechanics*, *812*, 1189–1212.

Brown, G. (2002). Henry Darcy and the making of a law. *Water Resources Research*, *38*(7), 1–12.

Brown, G. (2003). The history of the Darcy-Weisbach equation for pipe flow resistance. In J. R. Rogers & A. J. Fredrich (Eds.), *Proceedings from the ASCE Civil Engineering Conference and Exposition*, 2002, November 3–7, 2002, Washington, D.C., United States (pp. 34–43). https://doi.org/10.1061/9780784406502.fm

Brutsaert, W. (1965). A model for evaporation as a molecular diffusion process into a turbulent atmosphere. *Journal of Geophysical Research*, *70*(20), 5017–5024.

Brutsaert, W. (1982). *Evaporation into the atmosphere: Theory, history, and applications*. Dordrecht, Holland: Reidel Co.

Brutsaert, W. (2005). *Hydrology: An Introduction*. Cambridge, England: Cambridge University Press.

Buckingham, E. (1914). On physically similar systems: Illustrations of the use of dimensional equations. *Physical Review*, *4*(4), 345–376.

Businger, J., & Yaglom, A. (1971). Introduction to Obukhov's paper on 'turbulence in an atmosphere with a non-uniform temperature'. *Boundary-Layer Meteorology*, *2*(1), 3–6.

Calzetta, E. (2009). Friction factor for turbulent flow in rough pipes from Heisenberg's closure hypothesis. *Physical Review E*, *79*(5), 056311.

Chézy, A. (1775). Memoire sur la vitesse de l'eau conduit dans une rigole donne. *Dossier*, *847*, 363–368.

Chow, V. T. (Ed.). (1959). *Open Channel hydraulics*. New York, NY: McGraw-Hill.

D'arcy, W. T. (1915). Galileo and the principle of similitude. *Nature*, *95*(2381), 426.

Drazin, P. G., & Reid, W. H. (2004). *Hydrodynamic stability*. Cambridge, England: Cambridge University Press.

Foken, T. (2006). 50 years of the Monin–Obukhov similarity theory. *Boundary-Layer Meteorology*, *119*(3), 431–447.

French, R. H. (1985). *Open-channel hydraulics*. New York, NY: McGraw-Hill.

Frisch, U. (Ed.). (1995). *Turbulence*. Cambridge, England: Cambridge University Press.

Gioia, G., & Bombardelli, F. (2002). Scaling and similarity in rough channel flows. *Physical Review Letters*, *88*, 014501.

Gioia, G., & Chakraborty, P. (2006). Turbulent friction in rough pipes and the energy spectrum of the phenomenological theory. *Physical Review Letters*, *96*, 044502.

Gioia, G., Guttenberg, N., Goldenfeld, N., & Chakraborty, P. (2010). Spectral theory of the turbulent mean-velocity profile. *Physical Review Letters*, *105*(18), 184501.

Gleick, J. (2011). *Chaos: Making a new science*. London, England: Open Road Media.

Goldenfeld, N. (2006). Roughness-induced critical phenomena in a turbulent flow. *Physical Review Letters*, *96*(4), 044503.

Goldenfeld, N., & Shih, H. (2017). Turbulence as a problem in non-equilibrium statistical mechanics. *Journal of Statistical Physics*, *167*(3–4), 575–594.

Guttenberg, N., & Goldenfeld, N. (2009). Friction factor of two-dimensional rough-boundary turbulent soap film flows. *Physical Review E*, *79*(6), 065306.

Huthoff, F., Augustijn, D., & Hulscher, S. (2007). Analytical solution of the depth-averaged flow velocity in case of submerged rigid cylindrical vegetation. *Water Resources Research*, *43*(6). https://doi.org/10.1029/2006WR005625

Kader, B., & Yaglom, A. (1990). Mean fields and fluctuation moments in unstably stratified turbulent boundary layers. *Journal of Fluid Mechanics*, *212*, 637–662.

Kaimal, J. C., & Finnigan, J. J. (1994). *Atmospheric boundary layer flows: Their structure and measurement*. Oxford, England: Oxford University Press.

Katul, G., & Chu, C.-R. (1998). A theoretical and experimental investigation of energy-containing scales in the dynamic sublayer of boundary-layer flows. *Boundary-Layer Meteorology*, *86*(2), 279–312.

Katul, G., Hsieh, C.-I., & Sigmon, J. (1997). Energy-inertial scale interactions for velocity and temperature in the unstable atmospheric surface layer. *Boundary-Layer Meteorology*, *82*(1), 49–80.

Katul, G., Konings, A., & Porporato, A. (2011). Mean velocity profile in a sheared and thermally stratified atmospheric boundary layer. *Physical Review Letters*, *107*(26), 268502.

Katul, G., Li, D., Chamecki, M., & Bou-Zeid, E. (2013). Mean scalar concentration profile in a sheared and thermally stratified atmospheric surface layer. *Physical Review E*, *87*(2), 023004.

Katul, G., Li, D., Liu, H., & Assouline, S. (2016). Deviations from unity of the ratio of the turbulent Schmidt to Prandtl numbers in stratified atmospheric flows over water surfaces. *Physical Review Fluids*, *1*(3), 034401.

Katul, G., & Liu, H. (2017a). A Kolmogorov-Brutsaert structure function model for evaporation into a turbulent atmosphere. *Water Resources Research*, *53*(5), 3635–3644.

Katul, G., & Liu, H. (2017b). Multiple mechanisms generate a universal scaling with dissipation for the air-water gas transfer velocity. *Geophysical Research Letters*, *44*(4), 1892–1898.

Katul, G., Mammarella, I., Grönholm, T., & Vesala, T. (2018). A structure function model recovers the many formulations for air-water gas transfer velocity. *Water Resources Research*, *54*(9), 5905–5920.

Katul, G., & Manes, C. (2014). Cospectral budget of turbulence explains the bulk properties of smooth pipe flow. *Physical Review E*, *90*, 063008.

Katul, G., Manes, C., Porporato, A., Bou-Zeid, E., & Chamecki, M. (2015). Bottlenecks in turbulent kinetic energy spectra predicted from structure function inflections using the von Kármán-Howarth equation. *Physical Review E*, *92*(3), 033009.

Katul, G., Porporato, A., Shah, S., & Bou-Zeid, E. (2014). Two phenomenological constants explain similarity laws in stably stratified turbulence. *Physical Review E*, *89*(1), 023007.

Katul, G., Wiberg, P., Albertson, J. D., & Hornberger, G. (2002). A mixing layer theory for flow resistance in shallow streams. *Water Resources Research*, *38*, 1–8.

Katul, G. G., Porporato, A., Manes, C., & Meneveau, C. (2013). Co-spectrum and mean velocity in turbulent boundary layers. *Physics of Fluids*, *25*(9), 091702.

Kellay, H., Tran, T., Goldburg, W., Goldenfeld, N., Gioia, G., & Chakraborty, P. (2012). Testing a missing spectral link in turbulence. *Physical Review Letters*, *109*(25), 254502.

Keulegan, G. H. (1938). *Laws of turbulent flow in open channels* (Vol. 21, pp. 707–741). Gaithersburg, MD: National Bureau of Standards US.

Kolmogorov, A. (1941a). Dissipation of energy under locally isotropic turbulence. *Doklady Akademiia Nauk SSSR*, *32*, 16–18.

Kolmogorov, A. (1941b). The local structure of turbulence in incompressible viscous fluid for very large Reynolds numbers. *Doklady Akademiia Nauk SSSR*, *30*, 299–303.

Kolmogorov, A. (1962). A refinement of previous hypotheses concerning the local structure of turbulence in a viscous incompressible fluid at high Reynolds number. *Journal of Fluid Mechanics*, *13*(1), 82–85.

Konings, A., Katul, G., & Thompson, S. (2012). A phenomenological model for the flow resistance over submerged vegetation. *Water Resources Research*, *48*(2). https://doi.org/10.1029/2011WR011000

Kubo, R. (1966). The fluctuation-dissipation theorem. *Reports on Progress in Physics*, *29*(1), 255–284.

Lemons, D. S. (2018). *Dimensional analysis for curious undergraduates: A student's guide to dimensional analysis*. Cambridge, MA: Cambridge University Press.

Li, D., Katul, G., & Bou-Zeid, E. (2012). Mean velocity and temperature profiles in a sheared diabatic turbulent boundary layer. *Physics of Fluids*, *24*(10), 105105.

Li, D., Katul, G., & Bou-Zeid, E. (2015). Turbulent energy spectra and cospectra of momentum and heat fluxes in the stable atmospheric surface layer. *Boundary-Layer Meteorology*, *157*(1), 1–21.

Li, D., & Katul, G. G. (2017). On the linkage between the $k^{-5/3}$ spectral and $k^{-7/3}$ cospectral scaling in high-Reynolds number turbulent boundary layers. *Physics of Fluids*, *29*(6), 065108.

Li, D., Katul, G. G., & Zilitinkevich, S. S. (2015). Revisiting the turbulent Prandtl number in an idealized atmospheric surface layer. *Journal of the Atmospheric Sciences*, *72*(6), 2394–2410.

Li, D., Salesky, S., & Banerjee, T. (2016). Connections between the Ozmidov scale and mean velocity profile in stably stratified atmospheric surface layers. *Journal of Fluid Mechanics*, *797*, R3. https://doi.org/10.1017/jfm.2016.311

Lorenz, E. N. (1963). Deterministic nonperiodic flow. *Journal of the Atmospheric Sciences*, *20*(2), 130–141.

Manes, C., & Brocchini, M. (2015). Local scour around structures and the phenomenology of turbulence. *Journal of Fluid Mechanics*, *779*, 309–324.

Manes, C., Ridolfi, L., & Katul, G. (2012). A phenomenological model to describe turbulent friction in permeable-wall flows. *Geophysical Research Letters*, *39*(14). https://doi.org/10.1029/2012GL052369

Manning, R. (1891). On the flow of water in open channels and pipes. *Transactions of the Institution of Civil Engineers of Ireland*, *20*, 161–207.

McColl, K. A., Katul, G. G., Gentine, P., & Entekhabi, D. (2016). Mean-velocity profile of smooth channel flow explained by a cospectral budget model with wall-blockage. *Physics of Fluids*, *28*(3), 035107.

McColl, K. A., van Heerwaarden, C. C., Katul, G. G., Gentine, P., & Entekhabi, D. (2017). Role of large eddies in the breakdown of the Reynolds analogy in an idealized mildly unstable atmospheric surface layer. *Quarterly Journal of the Royal Meteorological Society*, *143*(706), 2182–2197.

Mehrafarin, M., & Pourtolami, N. (2008). Intermittency and rough-pipe turbulence. *Physical Review E*, *77*(5), 055304.

Merlivat, L. (1978). The dependence of bulk evaporation coefficients on air-water interfacial conditions as determined by the isotopic method. *Journal of Geophysical Research: Oceans*, *83*(C6), 2977–2980.

Monin, A., & Obukhov, A. (1954). Basic laws of turbulent mixing in the surface layer of the atmosphere. *Trudy Geofiz, Instituta Akademii Nauk, SSSR*, *24*(151), 163–187.

Moody, L. (1944). Friction factors for pipe flow. *Transactions of the ASME*, *66*, 671–684.

Pomeau, Y. (2016). The long and winding road. *Nature Physics*, *12*(3), 198–199.

Pope, S. B. (Ed.). (2000). *Turbulent flows*. Cambridge, England: Cambridge Univeristy Press.

Rayleigh, L. (1915). The principle of similitude. *Nature*, *95*, 66–68.

Richardson, L. F. (1922). *Weather prediction by numerical methods*. Cambridge, England: Cambridge University Press.

Salesky, S., Katul, G., & Chamecki, M. (2013). Buoyancy effects on the integral lengthscales and mean velocity profile in atmospheric surface layer flows. *Physics of Fluids*, *25*(10), 105101.

Succi, S. (2001). *The lattice Boltzmann equation: For fluid dynamics and beyond*. Oxford, England: Oxford University Press.

Tennekes, H., & Lumley, J. L. (1972). *A first course in turbulence*. Cambridge, MA: MIT press.

Townsend, A. (1976). *The structure of turbulent shear flow*. Cambridge, MA: Cambridge University Press.

Tran, T., Chakraborty, P., Guttenberg, N., Prescott, A., Kellay, H., Goldburg, W., … Gioia, G. (2010). Macroscopic effects of the spectral structure in turbulent flows. *Nature Physics*, *6*(6), 438–441.

Willcocks, W., & Holt, R. (Eds.). (1899). *Elementary hydraulics*. Cairo, Egypt: National Printing Office.

How to cite this article: Katul G, Li D, Manes C. A primer on turbulence in hydrology and hydraulics: The power of dimensional analysis. *WIREs Water*. 2019;e1336. https://doi.org/10.1002/wat2.1336